Vertical stress history and paleoburial in foreland basins unravelled by stylolite roughness paleopiezometry: Insights from bedding-parallel stylolites in the Bighorn Basin, Wyoming, USA.

Nicolas Beaudoin [a,*], Olivier Lacombe [b], Daniel Koehn [c], Marie-Eléonore David [b], Natalie Farrell [d], David Healy [d]

[a] Université de Pau et des Pays de l'Adour, E2S UPPA, CNRS, TOTAL, LFCR, Pau, France
[b] Sorbonne Université, CNRS-INSU, Institut des Sciences de la Terre de Paris, ISTeP UMR 7193, F-75005, Paris, France
[c] GeoZentrum Nordbayern, University Erlangen-Nuremberg, Schlossgarten 5, 91054, Erlangen, Germany
[d] School of Geosciences, King's College, University of Aberdeen, Aberdeen, AB24 3UE, UK

A B S T R A C T

We apply the stylolite roughness inversion technique on sedimentary, bedding-parallel stylolites hosted in the Paleozoic carbonates of the Bighorn and Madison formations cropping out in the Bighorn Basin, Wyoming, USA. The inversion technique applied to bedding-parallel stylolites allows determination of the absolute magnitude of the vertical stress experienced at the time dissolution stops along the pressure-solution planes. At the basin scale, reconstructed vertical stress magnitudes range from 19 ± 2 MPa to 35 ± 4 MPa in the Bighorn Fm, and from 12 ± 2 MPa to 37 ± 4 MPa in the Madison Fm. Once converted into depth and compared with up-to-date basin models of burial and contractional history, the dataset highlights that bedding-parallel stylolites accommodated compaction from ca. 220 Ma until ca. 90 Ma, i.e. until stress build-up related to the Sevier contraction made the maximum horizontal principal stress high enough to overcome the vertical principal stress. This study is key to illustrate how stylolites can be used to consistently access paleoburial and to unravel both stress evolution and timing in foreland settings, and indicates that pressure-solution remains active throughout the carbonate deposition history.

1. Introduction

Reconstructing variations in burial depth of strata is a challenging but vital task to constrain depositional, thermal and tectonic histories of sedimentary basins (Beaudoin and Lacombe, 2018; Guidish et al., 1985; Yalcin et al., 1997). A simple but inaccurate approach consists in reconstructing the thickness of the overlying sedimentary column by estimating the amount of rock compaction and thickness of eroded strata. Lacombe et al. (2009) used paleopiezometric inversion of calcite twins to estimate maximum burial depth under the debatable assumptions that the maximum differential stress related to layer-parallel shortening prevailed at the maximum burial depth and that the upper crust is at frictional stress equilibrium (Lacombe, 2007). Beke et al. (2019) recently proposed a relationship between deformation depth and the typology of deformation bands, however authors states that the typology itself depends on the degree of fluid-rock interactions, limiting this method's applicability. More common methods that are used to assess paleoburial depth are low-temperature thermochronology and vitrinite reflectance (e.g., Naeser and McCulloh, 2012; Roure et al., 2010; Tissot et al., 1987; Yalcin et al., 1997). Fluid inclusion

microthermometry on microveins combined with burial models may also help assess depth and timing of burial of strata (e.g., Anders et al., 2014; Becker et al., 2010; English et al., 2003; Fall et al., 2012). The three approaches above rely upon assumptions on the past geothermal gradient. In areas possibly affected by uplift and erosion, like fold-and-thrust belts and foreland basins, it is strongly challenging to solve for both temperature and burial for each time interval, so that there is usually a lack of control on paleo-burial estimates. A tool that provides constraints on the paleo-burial of strata without any assumption on the past geothermal gradient would thus be a significant step forward (Beaudoin and Lacombe, 2018), allowing for cross-checking between approaches, and hence leading to a gain in accuracy.

Stylolites, that are represented by serrated surfaces mainly in carbonate rocks, are common features in sedimentary basins (Andrews and Railsback, 1997; Laronne Ben-Itzhak et al., 2014; Stockdale, 1922; Tavani et al., 2010; Toussaint et al., 2018). Stylolites develop by chemical dissolution under stress (Alvarez et al., 1978; Fletcher and Pollard, 1981; Koehn et al., 2007; Toussaint et al., 2018) and are an early mechanism of accommodation of deformation, either related to tectonic shortening or to burial. In the latter case, stylolites are primarily

---

* Corresponding author.
 E-mail address: nicolas.beaudoin@univ-pau.fr (N. Beaudoin).

seen as a markers of the amount of compaction (Bathurst, 1987; Koehn et al., 2007; Railsback, 1993). In order to enhance our reservoir prediction capability, for both industrial and societal sake, there is a growing interest to understand how stylolites develop, how they impact fluid flow, and how they affect reservoir properties of carbonate rocks (e.g. Baud et al., 2016; Bruna et al., 2019; Heap et al., 2018). Beyond this classical approach, it was proposed recently that stylolite roughness can be reliably used as a paleopiezometer (Ebner et al., 2009, 2010; Rolland et al., 2012, 2014; Schmittbuhl et al., 2004; Toussaint et al., 2018), paving the way to a temperature independent marker of the burial history of carbonate rocks. Indeed, the roughness along a stylolite track, i. e., the evolution of the difference in height of nearest neighbors, holds self-affine properties that can be linked to the magnitude of applied stress prevailing in the strata at the time the final roughness of the stylolite fossilized. Various methods were tested to validate the theory of the technique (Schmittbuhl et al., 2004; Ebner et al., 2009, 2010), but cases of application to geological problems remain limited (Beaudoin et al., 2016, Beaudoin et al., 2019; Bertotti et al., 2017; Ebner et al., 2009; Rolland et al., 2014), especially in basins where contractional tectonics occurred.

We take advantage of the well-documented burial history and sedimentological and structural framework of the Bighorn Basin (Wyoming, USA) to reconstruct the evolution of vertical stress magnitudes in sedimentary strata that underwent burial followed by the Sevier-Laramide contractional deformation (Amrouch et al., 2010; Amrouch et al., 2010; Barbier et al., 2012; Beaudoin et al., 2011; Beaudoin et al., 2012; Bellahsen et al., 2006; Carrapa et al., 2019; Craddock and van der Pluijm, 1999; DeCelles et al., 1991; Erslev and Koenig, 2009; Lovely et al., 2010; Neely and Erslev, 2009; Weil and Yonkee, 2012; Yonkee and Weil, 2015). In this context where absolute dating of calcite cements of tectonic veins constrains the timing of contractional tectonics in the sedimentary cover (Beaudoin et al., 2018, Beaudoin et al., 2019), we aim at illustrating the potential of the stylolite roughness inversion by addressing the questions of how deep, and for how long, pressure-solution along a population of sedimentary, bedding-parallel stylolites remained an efficient mechanism to accommodate vertical compaction and affected the evolution of the reservoir properties. We also question whether the tectonic history impacts such a record, and we

reconstruct the absolute magnitude of the maximum vertical stress, hence of the maximum paleodepth of burial within the basin at the onset of layer-parallel shortening related to the far-field Sevier contraction.

2. Geological setting and sampling strategy

The Bighorn Basin (Fig. 1) formed in response to the long-lasting subduction of the Farallon plate, first as part of a broad marine foreland basin related to the thin-skinned Sevier orogeny during Cretaceous to early Paleocene times, and subsequently as an endorheic basin within the thick-skinned Laramide province that developed craton-wards by Late Cretaceous to Paleogene times (Yonkee and Weil, 2015). The sedimentary history of the Bighorn Basin (BHB) has been extensively studied in order to (1) reconstruct the geodynamic evolution of the North American plate, and (2) understand its georesources potential, e. g. hydrocarbons and geothermal potential. The depocenter of the basin stacked up to 5.5 km of sediments (DeCelles, 2004; Fox and Dolton, 1996; May et al., 2013) since Cambrian times, mainly consisting of shales and sandstones since the Mesozoic (Fig. 1a). In this study, we are focusing on the Paleozoic section of the BHB, that crops out in basement-cored folds on the eastern and western edges of the basin (Fig. 1b and c). The Paleozoic succession of the BHB consists of the Cambrian sandstones, marls and shales alternation of the Flathead, Gros Ventre and Gallatin Formations, the Ordovician massive dolomites of the Bighorn Formation, the Devonian sandstones of the Three Forks and Jefferson Formations, the Mississippian dolostones and limestones of the Madison Formation overlain by the Pennsylvanian sandstones of the Amsden and Tensleep Formations, and by the Permian limestones of the Phosphoria Formation. The competent core of the sedimentary succession lies in the Bighorn- Phosphoria interval, where most of the previously published microstructural work was carried out (Amrouch et al., 2010, Amrouch et al., 2010; Beaudoin et al., 2012; Bellahsen et al., 2006; Neely and Erslev, 2009). Three systematic, bed-perpendicular joint/vein sets (opening mode I) are encountered at the basin scale (Beaudoin et al., 2014 and references therein). In sequence, the first set comprises joints/veins striking N110° (after unfolding), likely formed during layer-parallel shortening related to the Sevier contraction. The two other sets are related to the Laramide contraction: the oldest one
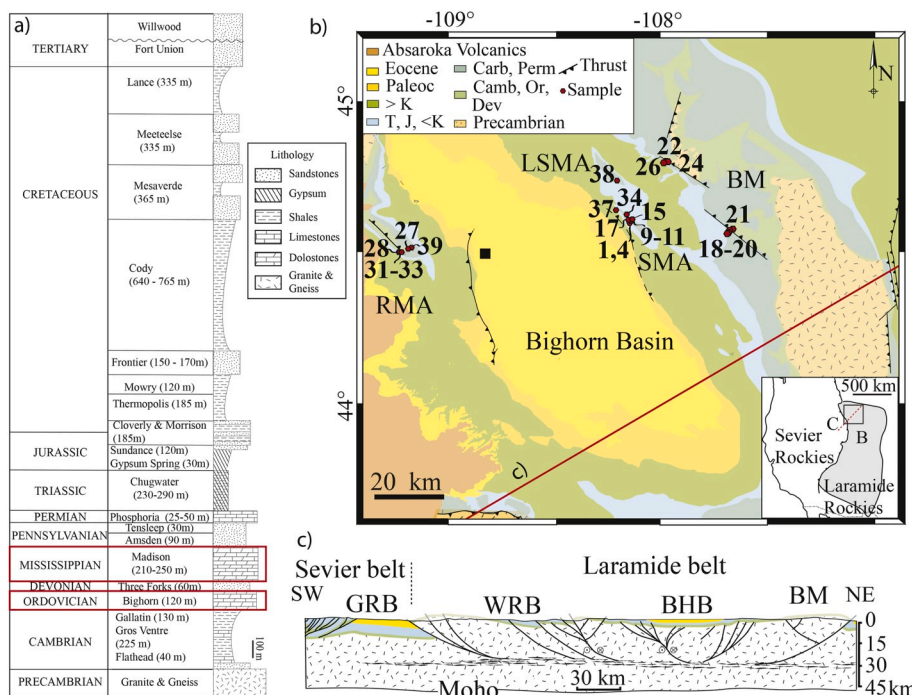
Fig. 1. a) stratigraphic column of the Bighorn Basin after Durdella (2001) and Neely and Erslev (2009), with reported thickness based on a well log located ~25 km west from Cody and located on the map b) by a black square. b) Simplified geological map of the Bighorn Basin, where are reported the locations of sampling sites as GPS numbers, see Table 1 for correspondence. Location of the area reported in the insert as a black frame labelled B. The red line on the map and the dotted red line in the insert locate the cross-section c). c) NE-SW cross section across the eastern Sevier Belt and northwestern Laramide belt (modified after Marshak et al. (2000); Lacombe and Bellahsen (2016)). Camb – Cambrian, Or – Ordovician, Dev – Devonian, Carb – Carboniferous, Perm – Permian, T - Triassic, J – Jurassic, <K – Lower Cretaceous, > K – Upper Cretaceous, RMA – Rattlesnake Mountain Anticline, LSMA – Little Sheep Mountain Anticline, SMA – Sheep Mountain Anticline, BM – Bighorn Mountains, GRB – Green River Basin, WRB – Wind River Basin, BHB – Bighorn Basin. (For interpretation of the references to colour in this figure legend, the reader is referred to the Web version of this article.)

comprises joints/veins striking N045° (after unfolding) and marks the Laramide layer-parallel shortening; the youngest one comprises joints/veins striking N135° that developed in response to outer-arc extension at the hinge of growing Laramide basement-cored folds (see Tavani et al., 2015 for a complete description of deformation patterns in folds and orogenic forelands). Absolute U–Pb ages from the calcite cements of these vein sets (Beaudoin et al., 2018) further suggest that Sevier-related veins developed earlier in the west (90 Ma) than in the east (75 Ma) of the basin while Laramide-related veins developed earlier in the east (72 Ma and 45 Ma) than in the west (60 Ma and 28 Ma) of the basin. Tectonic, bedding-perpendicular stylolites have also been described in the basin (Amrouch et al., 2010, Amrouch et al., 2010; Beaudoin et al., 2012, 2020); their peaks are mostly oriented ~ N110° and N045°, thus reflecting Sevier and Laramide layer-parallel shortening, respectively. Finally, mesoscale reverse and strike-slip faults have been extensively documented at the basin scale (Neely and Erslev, 2009; Amrouch et al., 2010, Amrouch et al., 2010; Beaudoin et al., 2012) and have also been interpreted as related to either Sevier or Laramide shortening.

Bedding-parallel stylolites were collected within 4 different basement-cored folds located in the BHB along an E-W transect (Fig. 1b and c): the Rattlesnake Mountain Anticline in the west, the Sheep Mountain and the Little Sheep Mountain Anticlines in the east, and the western part of the Bighorn Mountain arch that bounds the basin to the east. Because stylolite occurrence depends on lithology (e.g., Marshak and Engelder, 1985), sampling was limited to the dolomitic parts of the Bighorn and Madison Formations. We collected bedding-parallel, pre-folding sedimentary stylolites, the development of which is related to vertical compaction related to the burial of the strata (Fig. 2). Sedimentary facies were checked following the description established by Barbier et al. (2012) to ensure bedding-parallel stylolites were hosted by clay-poor dolomite of which dolomitization corresponds to the early deposition surface chemistry (eogenesis), i.e., predating burial and related stylolitisation (mesogenesis). That is important in order to limit the variability of mechanical and chemical parameters used for the stylolite roughness inversion. Hence samples were collected from the top of the Madison Formation, i.e. the Little Tongue and Bull Ridge members which are massive dolomite of which dolomitization occurred before stylolite development (Fig. 3c d). The Bighorn Formation represents pure dolomite that completely dolomitized before burial (Fig. 3e, Blackwelder, 1913). We collected samples in the top part of the Bighorn Formation at the two locations it crops out, the Rattlesnake Mountain Anticline and the Bighorn Mountains. We focused as much as possible on bedding-parallel stylolites showing a morphology of *suture and sharp peak* type (Fig. 3a b, Koehn et al., 2016), that have been shown to reflect the maximum burial depth experienced by the strata whilst the maximum principal stress (σ_1) was vertical (Beaudoin et al., 2019).

3. Stylolite roughness inversion for stress

The growth and the morphology of a stylolite are rate-dependent and are governed by the kinetics of dissolution (Stockdale, 1922) and by the distribution of heterogeneities, as well as by the amount of clay (Renard et al., 2001). Once dissolution starts, there is a thermodynamic competition between a destabilizing (roughening) force due to pinning particles on the stylolite surface that resist dissolution, and two stabilizing (smoothening) forces, long-range elastic forces and local surface tension, that tend to flatten the stylolite surface by preferentially dissolving areas of local roughness (Schmittbuhl et al., 2004). The inversion of the stylolite roughness exploits the self-affine properties of the stylolite roughness by treating it as a signal that is governed by two different processes according to the scale of observation (Schmittbuhl et al., 2004), i.e., the surface energy at small-scale (typically < 1 mm) and the elastic energy at larger scales. For all the stylolites that follow the growth model the method is valid for (Koehn et al., 2007), the spectral analysis of the roughness returns two different roughness exponents (Hurst exponents) (Schmittbuhl et al., 2004; Toussaint et al.,
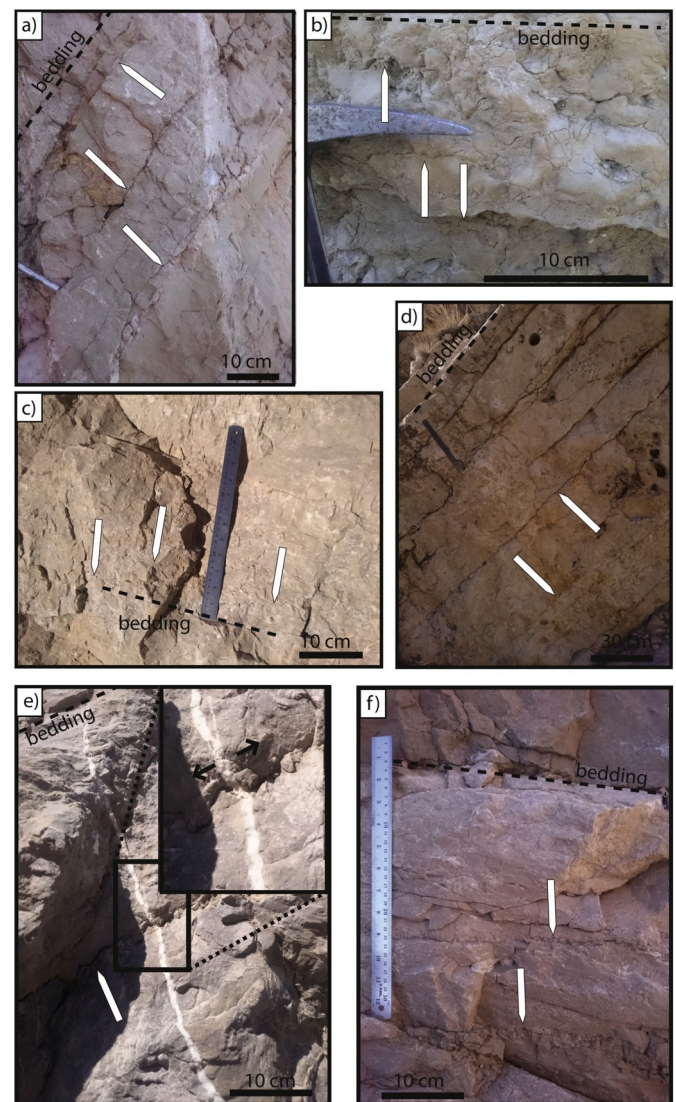

Fig. 2. Field photographs of bedding-parallel stylolites observed in the different structures and formations. Bedding is reported as a dotted black line, bedding-parallel stylolites are pointed out by white arrows, and the top of the pictures is up. a) Bighorn Mountains, Madison Formation. b) Bighorn Mountains, Bighorn Formation. c) Rattlesnake Mountain Anticline, Bighorn Formation. d) Rattlesnake Mountain Anticline, Madison Formation. e) Rattlesnake Mountain Anticline, Madison Formation, the insert shows the sequence between bedding-parallel stylolite and Sevier related tectonic vein. f) Sheep Mountain Anticline, Madison Formation.

2018). The scale at which there is a transition from one Hurst coefficient to another one is referred to as the cross-over length (Lc), and is analytically linked to the applied mean stress magnitude ($\sigma_m = \frac{\sigma_1+\sigma_2+\sigma_3}{3}$, in Pa) and differential stress magnitude ($\sigma_d = \sigma_1$-σ_3, in Pa), to the elastic parameters of the rock (Young modulus E (in Pa) and Poisson ratio) and to the solid-fluid interfacial energy γ (in J.m^{-2}) (Ebner et al., 2009; Schmittbuhl et al., 2004):

$$Lc = \frac{\gamma E}{\beta \sigma_m \sigma_d}. \tag{1}$$

where $\beta = \upsilon(1 - 2\upsilon)/\pi$, a dimensionless constant with υ being the Poisson ratio.

While the shape of a stylolite is affected by the strain rate and the stress orientation during its growth (Ebner et al., 2009; Koehn et al., 2012), the final roughness of a stylolite is a saturation state that is
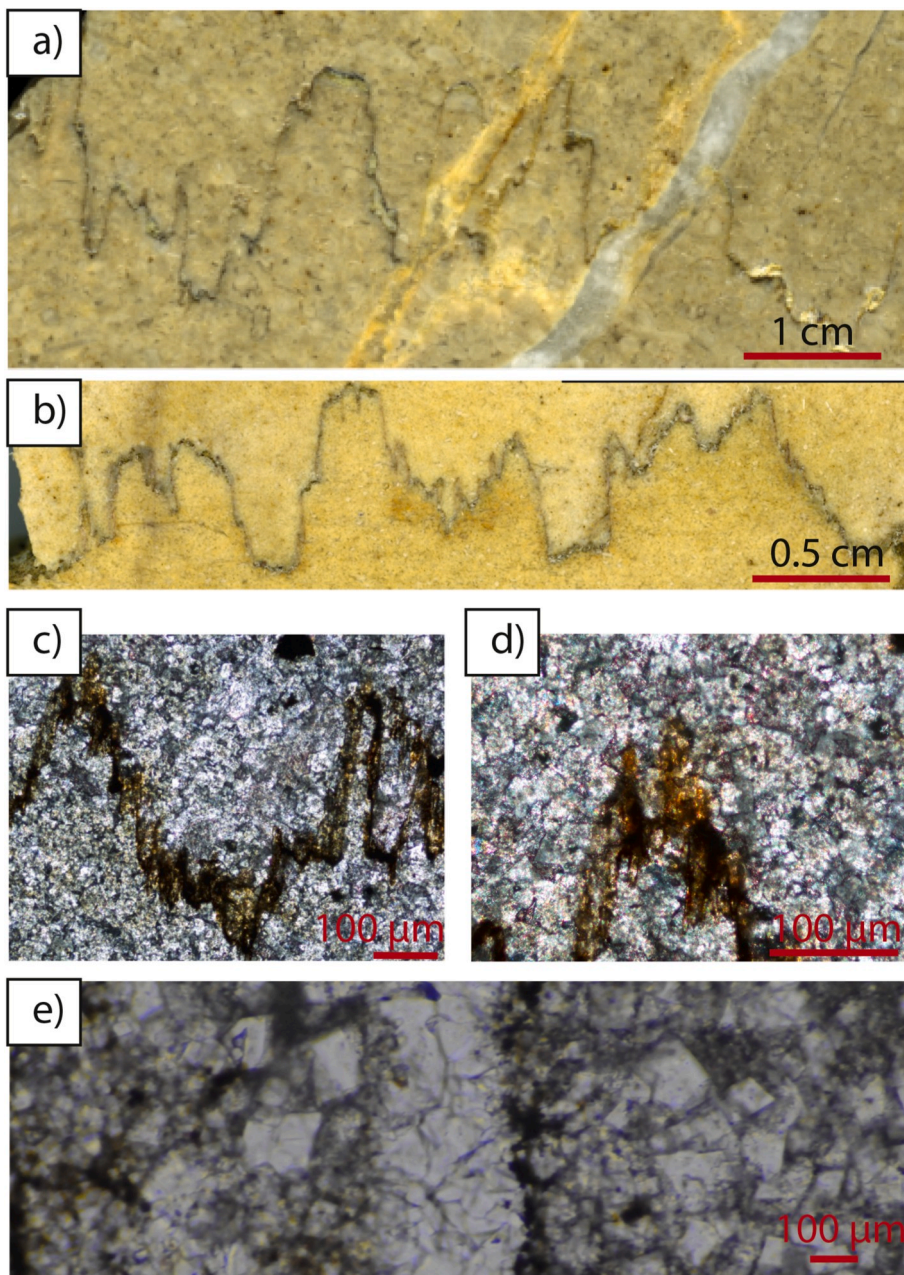
Fig. 3. a-b) High-resolution scans of polished slabs showing bedding-parallel stylolites, top of the strata is up. a) Scan of the sample RM-S26B, in the Madison Formation, that evidences that dissolution along the bedding-parallel stylolites predates development of tectonic vein. b) Scan of the sample LSM-S8, in the Madison Formation. c-e) microphotographs showing the texture of the host rock in the Madison Formation. (c, d at Sheep Mountain Anticline) and in the Bighorn Formation (e, in the Bighorn Mountains).

reached over a short period of time at the end of dissolution (Ebner et al., 2009; Rolland et al., 2012). Hence the final Hurst exponent that characterises the roughness of a stylolite is different from the width and the amplitude parameters of a stylolite that are related to the growth rate (Koehn et al., 2012) and to the amount of chemical compaction (e.g., Angheluta et al., 2012). The final stylolite roughness can be then treated as a snapshot of the prevailing ambient stress at the time it stopped being active (Schmittbuhl et al., 2004; Ebner et al., 2009; Rolland et al., 2012). Finally, as the dissolution occurs along a fluidic film, stylolite roughness inversion is not sensitive to the local fluid pressure, allowing to calculate the depth at which bedding-parallel stylolites stopped growing under a vertical maximum principal stress and using the average dry density of the overlying sandstones and carbonate rocks in the area (2.4 g cm^{-3}, Manger, 1963).

A number of studies explored in depth which signal analysis tool is the best for roughness inversion applied on stylolites. Three main methods can be used, the Fourier Power Spectrum, the Height

Correlation Function, and the Average Wavelet Coefficient (Ebner et al., 2009, 2010; Renard, 2004; Rolland et al., 2014; Schmittbuhl et al., 2004; Toussaint et al., 2018). For our study, we have chosen to conduct the signal analysis with the method that has proven to be the less impacted by sample number and quality: the Average Wavelet Coefficient (AWC) method with Daubechies D4 wavelets (Ebner et al., 2009; Simonsen et al., 1998). The AWC analysis reconstructs the signal as a sum of different wavelets, starting with a mother function (Simonsen et al., 1998), the scale a (mm) and the averaged wavelet coefficient W(a) being related as W(a) = a$^{(H+0.5)}$, where H is the roughness exponent, or Hurst exponent. AWC must return a Hurst exponent of 0.5 at the large scale and of 1.1 at the small-scale (Ebner et al., 2009; Rolland et al., 2014; Schmittbuhl et al., 2004; Toussaint et al., 2018).

In order to apply the stylolite roughness inversion for stress, samples were cut perpendicular to the stylolite planes. Stylolites with peaks that are oriented perpendicular to the solution planes were selected, then slabs were manually polished using abrasive mats from coarse (250 μm)

to extra fine (2.5 μm) in order to avoid alteration to the stylolite track. The stylolites were then scanned at a resolution of 12800 dpi using a commercial 2-D scanner. Stylolite tracks were hand drawn as 8 bits, 5 pt-thick pixelated lines using the drawing software GIMP (Fig. 4). The inversion process is using Matlab scripts that have been made available by Ebner et al. (2009) for AWC. The 1-D signal is then analyzed, and the consistency to the theory of the two governing processes is tested by fitting a non linear least squares regression through the signal (Ebner et al., 2009). We fix the slopes of the non-linear regression to the two theoretical Hurst exponents. When the stylolite roughness is consistent with the model, the script will return two slopes with a corresponding cross-over length Lc (Fig. 4a–b). Otherwise, the script will return a single slope with an extreme cross-over length value (Fig. 4c), that cannot be used for further stress inversion, the stylolite is then discarded. By applying this method on numerical signals, of which Hurst exponent and cross-over length were set beforehand, the error on determination of the cross over length due to the non-linear regression has been estimated around 23% (Rolland et al., 2014).

In the case of bedding-parallel-stylolites we assume a zero horizontal displacement in the stylolite plane, corresponding to a perfect isotropy of the horizontal principal stresses, such that $\sigma_v > \sigma_H \approx \sigma_h$ where σ_v, σ_H and σ_h are the absolute magnitude (i.e. without considering any effect related to fluid pressure) of the vertical principal stress, of the maximum horizontal principal stress and of the minimum horizontal principal stress, respectively. This leads to the simplification of equation (1) as follows

$$\sigma_v^2 = \frac{\gamma E}{\alpha Lc}. \tag{2}$$

with $\alpha = \frac{(1-2\nu)*(1+\nu)^2}{30\pi(1-\nu)^2}$ (Ebner et al., 2009). In order to obtain the vertical stress, we need to consider the appropriate values for the solid-fluid interfacial energy γ (J.m^{-2}), the Young modulus E and the Poisson ratio ν at the time the dissolution ended. For γ we used the known value for dolomite, $\gamma = 0.24$ J m^{-2} (Wright et al., 2001). For the mechanical parameters, we used the results of mechanical tests conducted on the most homogeneous, fracture-free samples of the Madison and Bighorn Formations that it was possible to collect. The tests on the Madison Formation were published elsewhere (Amrouch, 2010), and we produce new results for the Bighorn Formation (Supplementary Material). In nature and in the tests, the variability of the Poisson ratio is negligible for a given material, so we use the average value from the mechanical tests, i.e. 0.2 for the Madison Formation and 0.26 for the Bighorn Formation. We also use the average values returned by the tests for the Young modulus, i.e. 29 GPa for the Madison Formation and 43 GPa for the Bighorn Formation. It is noteworthy that the validity of the estimates of the Young modulus is more problematic as (1) it is highly variable in nature, even for a given material; (2) it shows some variability in the mechanical testing; and (3) it is expected to vary during the burial history. When considering all parameters the overall uncertainty on the stress value was estimated previously to ca. 12% (Rolland et al., 2014). Finally, the depth h is obtained using $\sigma_v = \rho g h$, with ρ the dry density (2.4 g cm^{-3}), and g the gravitational field acceleration (9.81 m s^{-2}). Here we consider the uncertainty on the depth to reflect the uncertainty on the stress estimate, i.e. 12%. As bedding-parallel stylolites can form at nearly any depth as long as the maximum principal stress is vertical, we consider a population of stylolites to be representative of the range of depths reached by the strata of interest.

4. Results

At the basin scale, inversion of stylolite roughness was successfully applied on 51 bedding-parallel stylolites (Rattlesnake Mountain, n = 12; Little Sheep Mountain-Sheep Mountain, n = 22; Bighorn Mountain, n = 17) out of the 58 stylolites tested (Table 1), that were hosted in the Madison Formation (n = 38) and in the Bighorn Formation (n = 13). The

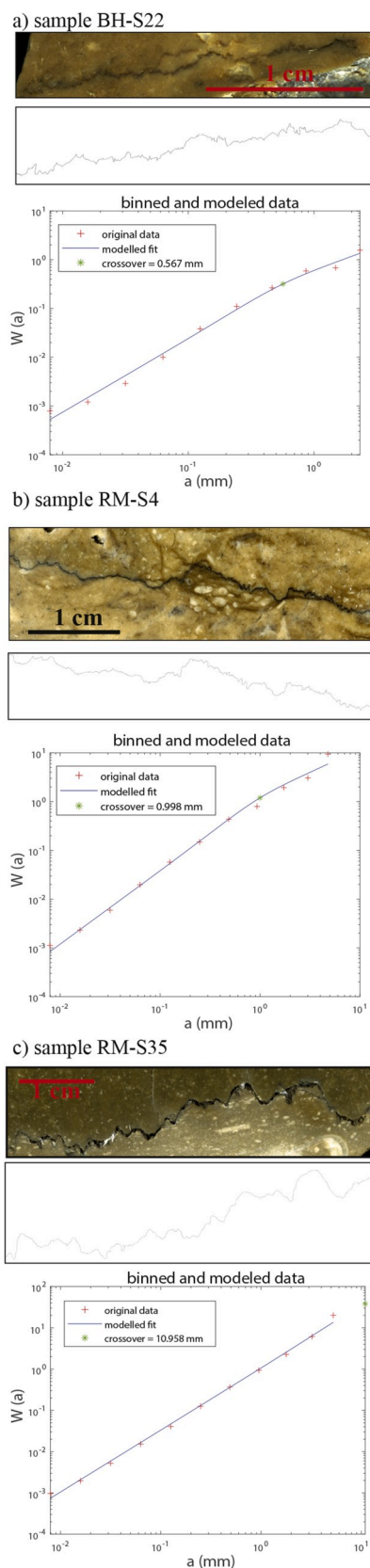

Fig. 4. Three examples of application of the stylolite roughness inversion technique. For each example given here the polished slab is scanned in 2D (top), then hand drawn with a 5 pixel-thick line (middle), then analyzed using an average wavelet spectrum method (bottom). See text for more details. Example c) illustrates a failure in the inversion process, since a single slope is derived.

distribution of vertical stress magnitudes at the basin-scale (Fig. 5) ranges (1) in the Bighorn Formation from 19 ± 2 MPa to 35 ± 4 MPa, corresponding to depths ranging from 800 ± 90 m to 1500 ± 170 m (median = 1104 m) and (2) in the Madison Formation from 12 ± 1.5 MPa to 37 ± 4 MPa, corresponding to depths ranging from 510 ± 60 m to 1570 ± 190 m (median = 850 m). At Rattlesnake Mountain Anticline, the

vertical stress ranges from 15 ± 2 MPa to 27 ± 3 MPa, corresponding to depths ranging from 930 ± 110 m to 1150 ± 140 m for the Bighorn Formation (median = 1060 m), and from 640 ± 80 m to 1150 ± 140 m for the Madison Formation (median = 720 m). At Little Sheep Mountain – Sheep Mountain Anticlines, the vertical stress ranges from 14 ± 1.5 MPa to 37 ± 4 MPa, corresponding to depths ranging from 640 ± 80 m to

Table 1
Sample name and location, and results from stylolite roughness inversion by average wavelet coefficient.

Name	GPS	Longitude	Latitude	Formation	Lc (mm)[a]	Vertical Stress (MPa)[b]	Depth (m)[b]
Rattlesnake Mountain Anticline							
RM-S1	27	−109.14789	44.511	Bighorn	1.466	22	934
RM-S3	27	−109.14789	44.511	Bighorn	0.921	27	1147
RM-S4	27	−109.14789	44.511	Bighorn	0.998	26	1104
RM-S5	27	−109.14789	44.511	Bighorn	1.15	24	1019
RM-S9	28	−109.19747	44.501	Madison	1.658	17	722
RM-S9-2	28	−109.19747	44.501	Madison	0.865	23	977
RM-S18	31	−109.19577	44.501	Madison	1.885	16	680
RM-S31	39	−109.13635	48.858	Madison	0.636	27	1147
RM-S26T	33	−109.1907	44.501	Madison	1.579	17	722
RM-S26B	33	−109.1907	44.501	Madison	2.103	15	637
RM S27	39	−109.1907	44.501	Madison	1.579	17	722
RM-S29	39	−109.13635	48.858	Madison	0.973	22	934
RM-S35	39	−109.13635	48.858	Madison	N.A.	N.A.	N.A.
Little Sheep Mountain Anticline							
LSM-S1	38	−108.19008	44.513	Madison	1.36	19	807
LSM-S2	38	−108.19008	44.513	Madison	0.572	29	1232
LSM-S3	38	−108.19008	44.513	Madison	0.759	25	1062
LSM-S4	38	−108.19008	44.513	Madison	0.972	22	934
LSM-S5	38	−108.19008	44.513	Madison	0.445	32	1359
LSM-S6	38	−108.19008	44.513	Madison	0.482	31	1317
LSM-S8-1	38	−108.19008	44.513	Madison	2.283	14	595
LSM-S8-2	38	−108.19008	44.513	Madison	0.838	24	1019
LSM-S14	38	−108.19008	44.513	Madison	1.673	17	722
LSM-S15	38	−108.19008	44.513	Madison	0.43	33	1402
LSM-S16	38	−108.19008	44.513	Madison	1.443	18	765
Sheep Mountain Anticline							
SM-S1	1	−108.13924	44.606	Madison	0.34	37	1572
SM-S5	4	−108.1384	44.61	Madison	0.639	27	1147
SM-S15	9	−108.13476	44.613	Madison	1.491	18	765
SM-S17	10	−108.13423	44.613	Madison	0.69	26	1104
SM-S18-1	11	−108.13403	44.613	Madison	0.88	23	977
SM-S18-2	11	−108.13403	44.613	Madison	0.912	23	977
SM-S18-3	11	−108.13403	44.613	Madison	1.748	16	680
SM-S6-1	17	−108.14007	44.611	Madison	0.336	37	1572
SM-S7	17	−108.14007	44.611	Madison	0.53	30	1274
SM-S11	17	−108.14007	44.611	Madison	1.043	21	892
SM-S26	34	−108.1434	44.625	Madison	1.504	18	765
Western Part of the Bighorn Mountain							
BM-S1	18	−107.70892	44.569	Madison	3.408	12	510
BM-S4-1	18	−107.70892	44.569	Madison	1.346	19	807
BM-S4-2	18	−107.70892	44.569	Madison	1.679	17	722
BM-S5-1	18	−107.70892	44.569	Madison	1.294	19	807
BM-S5-2	18	−107.70892	44.569	Madison	2.626	13	552
BM-S8	18	−107.70892	44.569	Madison	0.884	23	977
BM-S19	19	−107.70032	44.575	Madison	2.866	13	552
BM-S20	19	−107.70032	44.575	Madison	1.359	19	807
BM-S22	20	−107.69075	44.579	Bighorn	0.567	35	1487
BM-S25-1	21	−107.68891	44.579	Bighorn	1.118	25	1062
BM-S25-3	21	−107.68891	44.579	Bighorn	0.911	27	1147
BM-S25-2	21	−107.68891	44.579	Bighorn	0.584	34	1444
BM-S26-2	21	−107.68891	44.579	Bighorn	0.698	31	1317
BM-S27-1	21	−107.68891	44.579	Bighorn	1.144	24	1019
BM-S27-2	21	−107.68891	44.579	Bighorn	1.694	20	849
BM-S30	22	−107.96756	44.795	Bighorn	1.956	19	807
BM-S32	24	−107.9667	44.795	Bighorn	0.9	27	1147
BM-S21	20	−107.69075	44.579	Bighorn	N.A.	N.A.	N.A.
BM-S26-1	21	−107.68891	44.579	Bighorn	N.A.	N.A.	N.A.
BM-S28	21	−107.68891	44.579	Bighorn	N.A.	N.A.	N.A.
BM-S29	21	−107.68891	44.579	Bighorn	N.A.	N.A.	N.A.
BM-S35	24	−107.9667	44.795	Bighorn	N.A.	N.A.	N.A.
BM-S39	26	−107.96959	44.792	Madison	N.A.	N.A.	N.A.

[a] Crossover length Lc is given within 23%, N.A. represents samples for which the method failed (12% of the population).
[b] Vertical stress and depth values are given with 12% relative error.
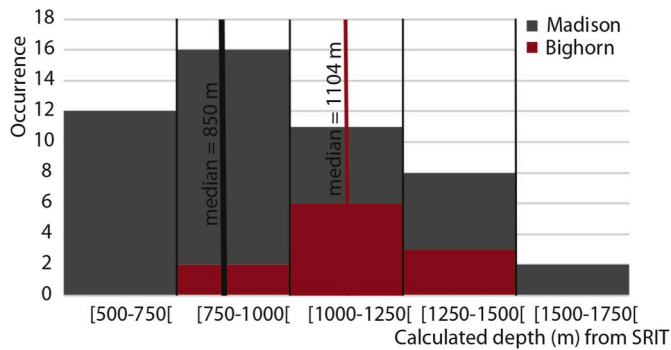
Fig. 5. Bar plot showing the distribution of the depth values obtained from stylolite roughness inversion of the bedding-parallel stylolites population at the basin-scale, irrespective of the fold structure where samples were collected. Depths related to bedding-parallel stylolites sampled in the Madison Formation are reported in grey while the ones coming from the Bighorn Formation are reported in red. – SRIT – Stylolite roughness inversion technique. (For interpretation of the references to colour in this figure legend, the reader is referred to the Web version of this article.)

1570 ± 190 m for the Madison Formation (median = 990 m). Finally, in the western flank of the Bighorn Mountains, the vertical stress ranges from 12 ± 1.5 MPa to 35 ± 4 MPa, corresponding to depths ranging from 800 ± 90 m to 1500 ± 170 m for the Bighorn Formation (median = 1147 m), and from 510 ± 60 m to 980 ± 120 m for the Madison Formation (median = 765 m) (Fig. 6). The success of the inversion process (88%) was tested regarding the morphological type of the stylolites, the percentage of failure being much higher for the *rectangular layer* and *seismogram pinning* types (40%, for both types) than for the *suture and sharp peak* type (6.5%). However, as the population is very small for both *rectangular layer* and *seismogram pinning* types (7 and 5, respectively), no definitive behaviour can be deduced from this study only.

5. Discussion

Stylolite roughness inversion was used to consistently estimate the maximum vertical stress experienced by dolomitic strata for as long as the vertical stress magnitude stayed higher than the horizontal stress magnitude, i.e. since early burial to Sevier - Laramide shortening. Our results show that the range of vertical stress values and so the burial

depths are similar for both considered formations (Fig. 5), and that the maximum depth at which bedding-parallel stylolites stopped being active is lower than the maximum depth predicted by the cumulated thickness of the overlying formations (Fox and Dolton, 1996; Neely and Erslev, 2009)(Fig. 6). Considering the median depth of the populations (Fig. 5), the stylolites from the Madison Formation recorded shallower depths (median = 850m) than the ones from the Bighorn Formation (median = 1104 m), *i.e.*, a difference of 250 m. Considering the median depth by structure (Table 1, Fig. 6), the difference is of 300 m in the Rattlesnake Mountain Anticline and of 300 m in the western flank of the Bighorn Mountains. These differences in depth are well in line with the thickness between the top of each formation estimated from the sedimentary column and well logs (~300 m, Fig. 1, Fox and Dolton, 1996; Durdella, 2001). Results of this study add up to the growing number of evidence that stylolite roughness inversion is a powerful tool to access paleoburial without any assumption on the past thermal gradient or fluid pressure (Ebner et al., 2009; Rolland et al., 2012; Beaudoin et al., 2016, Beaudoin et al., 2019; Bertotti et al., 2017; Beaudoin and Lacombe, 2018). Each of the depth values we obtained represents the stage at which some part of the stylolite population stopped being active (Toussaint et al., 2018). Consequently, the minimum depths recorded (from 500 to 800 m) correspond to the minimum depths at which the development of some bedding-parallel stylolites halted; in other words pressure solution likely started at burial depth shallower than 500m, even though the minimum depth required for stylolites formation still remains unknown. This illustrates that chemical compaction is a mechanism that can be active at very shallow depth (Ebner et al., 2009; Rolland et al., 2014), discarding theories that predict a minimum depth of 800 m to form bedding-parallel stylolites in the absence of clay-enhanced reactions (Finkel and Wilkinson, 1990 ; Railsback, 1993).

In order to discuss the timing and the duration of bedding-parallel stylolite development, we projected the range of calculated depths onto the burial models for the eastern and the western parts of the Bighorn basins proposed in Beaudoin et al., 2014 after May et al. (2013), based on well data and thermochronology (Fig. 6). The validity of this burial-exhumation model is supported by the recent burial models based on organic matter in the basin (Ellis et al., 2017; Gottardi et al., 2019).

The bedding-parallel stylolites we studied happen to show some clear field evidence that they developed prior to the formation of the tectonic, bed-perpendicular veins (Figs. 2 and 3), the orientations of which indicate that they are related to either Sevier contraction (~E-W
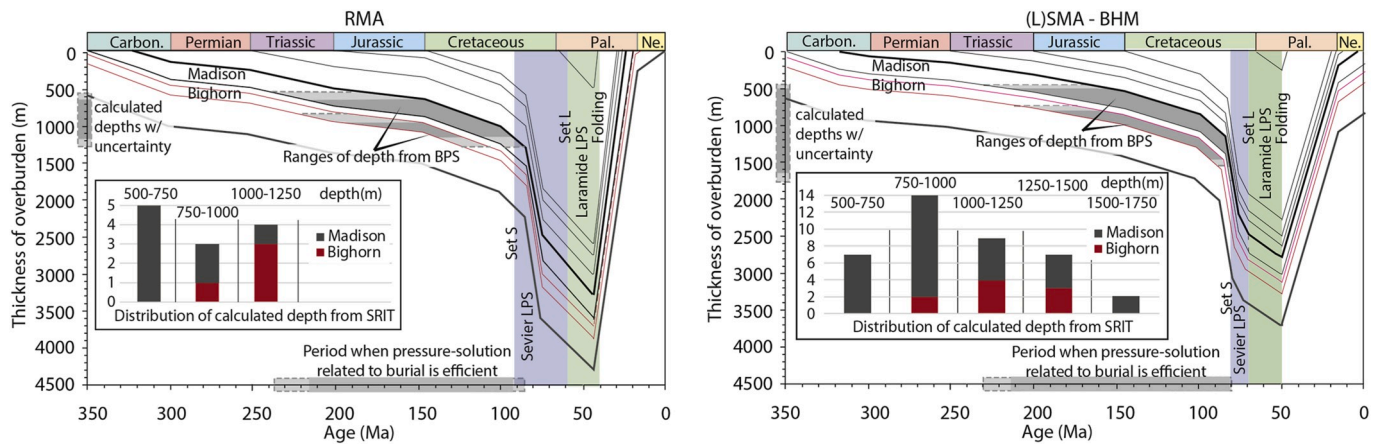
Fig. 6. Burial curves (modified after May et al. (2013), Beaudoin et al., 2014) valid for the western margin of the basin (left-hand side) and for the eastern margin of the basin (right-hand side). The absolute age of the development of the tectonic veins are reported after Beaudoin et al. (2018) as blue highlights (Sevier) and green highlights (Laramide). In each case, the range of depth obtained from applying the stylolite roughness inversion technique on the local population of bedding-parallel stylolites is reported on the y-axis and on the graph in the considered formations. Corresponding timing of activity for chemical compaction along bedding-parallel stylolites is projected on the x-axis. Uncertainties of ca. 12% are reported along as lighter grey area. Bar plots of the distribution of the depths vs the number of stylolite analyzed are reported for each side of the basin, with data from the Madison Formation in grey and data from the Bighorn Formation in red. (For interpretation of the references to colour in this figure legend, the reader is referred to the Web version of this article.)

to N110°E) or Laramide contraction (NE-SW) (Amrouch et al., 2010; Beaudoin et al., 2012; Bellahsen et al., 2006; Craddock and van der Pluijm, 1999; Varga, 1993). Therefore, one can safely consider that the bedding-parallel stylolites have developed prior to the Sevier and Laramide shortening, i.e., during burial and not during subsequent Paleogene exhumation.

The timing of opening of the Sevier and Laramide related veins in the studied structures has been set by means of U–Pb absolute dating (Beaudoin et al., 2018, Beaudoin et al., 2019) and is reported on the burial curves (Fig. 6). With respect to the fold structure and the formation considered, it appears that the maximum depths recorded by the bedding-parallel stylolites correspond to an age which is always older than, or equal to, the one of the development of tectonic veins related to Sevier layer-parallel shortening. This supports the results of the inversion as one can expect bedding-parallel stylolites have stopped being active when the maximum principal stress σ_1 switched from vertical to horizontal, as peaks of stylolites are parallel to the σ_1 orientation (e.g. Koehn et al., 2007). In the Bighorn Basin, the stress switch happened when the magnitude of the maximum horizontal stress transmitted forelandward from the Sevier front overcame the magnitude of the vertical stress related to burial. We can estimate that this switch from vertical to horizontal maximum principal stress occurred for an absolute value of at least 35 ± 4 MPa.

Paleopiezometric studies of calcite twinning in the Madison Formation at the Sheep Mountain Anticline (Amrouch et al., 2010a, 2010b) and at the Rattlesnake Mountain Anticline (Beaudoin et al., 2012) documented differential stress ($\sigma_1 - \sigma_3$) magnitudes, values of the stress ratio $\left(\phi = (\sigma_2 - \sigma_3)/(\sigma_1 - \sigma_3) \right)$, and stress regimes prevailing in the rocks during the Sevier layer-parallel shortening. From these data, it is possible to derive the absolute magnitude of σ_1 if we set the depth of deformation. Considering the range of burial depths valid at Sheep Mountain Anticline during the Sevier layer-parallel shortening, as given by the absolute age of the tectonic veins projected on the burial model (Fig. 6), we can estimate that the absolute magnitude of σ_1 ranges from 55 ± 10 MPa at the minimum depth (1500 m) to 79 ± 10 MPa at the maximum depth (2500 m). At the Rattlesnake Mountain Anticline, the same approach yields absolute magnitude of σ_1 ranging from 65 ± 7 MPa at minimum depth (1300 m) to 100 ± 7 MPa at maximum depth (2800 m). A more recent paleopiezometric study based on tectonic stylolite roughness inversion in the Madison Formation at the Sheep-Little Sheep Mountain Anticlines (Beaudoin et al., 2020) further provides absolute magnitudes of the maximum horizontal principal stress σ_1 related to the Sevier layer-parallel shortening ranging from 50 ± 2 MPa at minimum depth (1500 m) to 67 ± 5 MPa at maximum depth (2500 m). All these independent estimates indicate that the absolute magnitudes of the maximum horizontal principal stress σ_1 associated with calcite twinning and tectonic-related pressure solution related to the Sevier contraction were consistently higher than the one (35 ± 4 MPa) recorded at the time σ_1 switched from vertical to horizontal. The present study therefore reveals that the Sevier-related maximum horizontal principal stress increased faster than the vertical stress related to burial during orogenic stress loading. This is consistent with a regional stress build-up model, with the maximum horizontal stress expectedly overcoming the vertical stress by a margin before being able to trigger anisotropic deformation such as joints/veins and stylolites. Furthermore, our study supports that the orogenic stress build-up was rather fast since there is little time (~5 Ma, Fig. 6) between the activity of the last bedding-parallel stylolite and the opening of the first Sevier-related tectonic vein.

Finally, our results indicate that the investigated bedding-parallel stylolite population was active at least from, and likely before, ca. 240 Ma ago until 85 Ma ago in the western part of the basin, and at least from, and likely before, 230 Ma ago until 80 Ma ago in the eastern part of the basin (Fig. 5). By comparing the paleodepth to the burial curve, we can provide for the first time a time bracket for the expected long-lasting development of a population of bedding-parallel stylolites. Such information is of importance when it comes to reservoir property evolution during burial, as stylolites have a strong influence on the porosity, permeability and mechanical properties of carbonates (Aharonov and Karcz, 2019; Bruna et al., 2019; Martín-Martín et al., 2018; Toussaint et al., 2018).

6. Conclusions

This study uses stylolite roughness paleopiezometry to constrain the magnitude of the vertical stress and the burial depth of selected strata during the foreland evolution of the Bighorn Basin, Wyoming, USA. The results show that the paleopiezometric analysis of the roughness of a relatively small population (n = 51) of bedding-parallel stylolites can reliably return the pre-shortening burial evolution over a long period of time (~150 Ma). Bedding-parallel stylolites also yield the depth and timing at which the maximum principal stress switched orientation from burial-related vertical to orogenic contraction-related horizontal, both being supported by the available absolute ages of the kinematically compatible tectonic veins. Beyond regional implications, this study illustrates the potential of the inversion of the bedding-parallel stylolite roughness, conducted with a wavelet analyses, as a reliable and powerful paleopiezometric tool for basin and structural analyses, allowing for paleoburial estimates independently of past geothermal gradients, and adding important information about the timing of orogenic stress build-up in orogenic forelands.

Declaration of competing interest

The authors declare that they have no known competing financial interests or personal relationships that could have appeared to influence the work reported in this paper.

CRediT authorship contribution statement

Nicolas Beaudoin: Conceptualization, Investigation, Methodology, Formal analysis, Data curation, Writing - original draft. **Olivier Lacombe:** Conceptualization, Data curation, Writing - original draft, Writing - review & editing, Funding acquisition. **Daniel Koehn:** Conceptualization, Methodology, Writing - original draft, Writing - review & editing, Funding acquisition. **Marie-Eléonore David:** Data curation. **Natalie Farrell:** Data curation, Writing - original draft, Writing - review & editing. **David Healy:** Writing - review & editing.

Appendix A. Supplementary data

Supplementary data to this article can be found online at https://doi.org/10.1016/j.jsg.2020.104061.

References

Aharonov, E., Karcz, Z., 2019. How stylolite tips crack rocks. J. Struct. Geol. 118, 299–307.

Alvarez, W., Engelder, T., Geiser, P.A., 1978. Classification of solution cleavage in pelagic limestones. Geology 6, 263–266.

Amrouch, K., 2010. Apport de l'analyse microstructurale à la compréhension des mécanismes de plissement: Exemples de structures plissées aux USA (Wyoming) et en Iran (Zagros). UPMC, Paris, p. 479.

Amrouch, K., Lacombe, O., Bellahsen, N., Daniel, J.-M., Callot, J.-P., 2010. Stress and strain patterns, kinematics and deformation mechanisms in a basement-cored anticline: Sheep Mountain Anticline, Wyoming. Tectonics 29, TC1005.

Amrouch, K., Robion, P., Callot, J.P., Lacombe, O., Daniel, J.M., Bellahsen, N., Faure, J. L., 2010. Constraints on deformation mechanisms during folding provided by rock physical properties: a case study at Sheep Mountain anticline (Wyoming, USA). Geophys. J. Int. 182, 1105–1123.

Anders, M.H., Laubach, S.E., Scholz, C.H., 2014. Microfractures: a review. J. Struct. Geol. 69, 377–394.

Andrews, L.M., Railsback, L.B., 1997. Controls on stylolite development: morphologic, lithologic, and temporal evidence from bedding-parallel and transverse stylolites from the US Appalachians. J. Geol. 105, 59–73.

Angheluta, L., Mathiesen, J., Aharonov, E., 2012. Compaction of porous rock by dissolution on discrete stylolites: a one-dimensional model. J. Geophys. Res.: Solid Earth 117, B08203.

Barbier, M., Hamon, Y., Callot, J.-P., Floquet, M., Daniel, J.-M., 2012. Sedimentary and diagenetic controls on the multiscale fracturing pattern of a carbonate reservoir: the Madison Formation (Sheep Mountain, Wyoming, USA). Mar. Petrol. Geol. 29, 50–67.

Bathurst, R.G., 1987. Diagenetically enhanced bedding in argillaceous platform limestones: stratified cementation and selective compaction. Sedimentology 34, 749–778.

Baud, P., Rolland, A., Heap, M., Xu, T., Nicolé, M., Ferrand, T., Reuschlé, T., Toussaint, R., Conil, N., 2016. Impact of stylolites on the mechanical strength of limestone. Tectonophysics 690, 4–20.

Beaudoin, N., Bellahsen, N., Lacombe, O., Emmanuel, L., 2011. Fracture-controlled paleohydrogeology in a basement-cored, fault-related fold: Sheep Mountain Anticline, Wyoming, United States. G-cubed 12, Q06011.

Beaudoin, N., Bellahsen, N., Lacombe, O., Emmanuel, L., Pironon, J., 2014. Crustal-scale fluid flow during the tectonic evolution of the Bighorn Basin (Wyoming, USA). Basin Res. 26, 403–435.

Beaudoin, N., Gasparrini, M., David, M.E., Lacombe, O., Koehn, D., 2019. Bedding-parallel stylolites as a tool to unravel maximum burial depth in sedimentary basins: application to Middle Jurassic carbonate reservoirs in the Paris basin, France. GSA Bull. 131, 1239–1254.

Beaudoin, N., Koehn, D., Lacombe, O., Lecouty, A., Billi, A., Aharonov, E., Parlangeau, C., 2016. Fingerprinting stress: stylolite and calcite twinning paleopiezometry revealing the complexity of progressive stress patterns during folding-The case of the Monte Nero anticline in the Apennines, Italy. Tectonics 35, 1687–1712.

Beaudoin, N., Lacombe, O., 2018. Recent and future trends in paleopiezometry in the diagenetic domain: insights into the tectonic paleostress and burial depth history of fold-and-thrust belts and sedimentary basins. J. Struct. Geol. 114, 357–365.

Beaudoin, N., Lacombe, O., Bellahsen, N., Amrouch, K., Daniel, J.-M., 2014. Evolution of pore-fluid pressure during folding and basin contraction in overpressured reservoirs: insights from the Madison–Phosphoria carbonate formations in the Bighorn Basin (Wyoming, USA). Mar. Petrol. Geol. 55, 214–229.

Beaudoin, N., Lacombe, O., David, M.E., Koehn, D., 2020. Does stress transmission in forelands depend on structural style ? Distinctive stress magnitudes during Sevier thin-skinned and Laramide thick-skinned layer-parallel shortening in the Bighorn Basin (USA) revealed by stylolite and calcite twinning paleopiezometry. Terra. Nova. https://doi.org/10.1111/ter.12451.

Beaudoin, N., Lacombe, O., Roberts, N.M.W., Koehn, D., 2018. U-Pb dating of calcite veins reveals complex stress evolution and thrust sequence in the Bighorn Basin, Wyoming, USA. Geology 46, 1015–1018.

Beaudoin, N., Lacombe, O., Roberts, N.M.W., Koehn, D., 2019. U-Pb dating of calcite veins reveals complex stress evolution and thrust sequence in the Bighorn Basin, Wyoming, USA: REPLY. Geology 47, e481.

Beaudoin, N., Leprêtre, R., Bellahsen, N., Lacombe, O., Amrouch, K., Callot, J.-P., Emmanuel, L., Daniel, J.-M., 2012. Structural and microstructural evolution of the Rattlesnake Mountain Anticline (Wyoming, USA): new insights into the sevier and Laramide orogenic stress build-up in the Bighorn basin. Tectonophysics 576–577, 20–45.

Becker, S.P., Eichhubl, P., Laubach, S.E., Reed, R.M., Lander, R.H., Bodnar, R.J., 2010. A 48 m.y. history of fracture opening, temperature, and fluid pressure: Cretaceous Travis Peak Formation, East Texas basin. Geol. Soc. Am. Bull. 122, 1081–1093.

Beke, B., Fodor, L., Millar, L., Petrik, A., 2019. Deformation band formation as a function of progressive burial: depth calibration and mechanism change in the Pannonian Basin (Hungary). Mar. Petrol. Geol. 105, 1–16.

Bellahsen, N., Fiore, P., Pollard, D.D., 2006. The role of fractures in the structural interpretation of Sheep Mountain Anticline, Wyoming. J. Struct. Geol. 28, 850–867.

Bertotti, G., de Graaf, S., Bisdom, K., Oskam, B., Vonhof, B.H., Bezerra, H.R., Reijmer, F. J.G., L, J., Cazarin, C., 2017. Fracturing and fluid-flow during post-rift subsidence in carbonates of the Jandaíra formation, Potiguar basin, NE Brazil. Basin Res. 29, 836–853.

Blackwelder, E., 1913. Origin of the Bighorn dolomite of Wyoming. Bull. Geol. Soc. Am. 24, 607–624.

Bruna, P.-O., Lavenu, A.P., Matonti, C., Bertotti, G., 2019. Are stylolites fluid-flow efficient features? J. Struct. Geol. 125, 270–277.

Carrapa, B., DeCelles, P.G., Romero, M., 2019. Early inception of the Laramide orogeny in Southwestern Montana and Northern Wyoming: implications for models of flat-slab subduction. J. Geophys. Res.: Solid Earth 124, 2102–2123.

Craddock, J.P., van der Pluijm, B.A., 1999. Sevier–Laramide deformation of the continental interior from calcite twinning analysis, west-central North America. Tectonophysics 305, 275–286.

DeCelles, P.G., 2004. Late Jurassic to Eocene evolution of the Cordilleran thrust belt and foreland basin system, western USA. Am. J. Sci. 304, 105–168.

DeCelles, P.G., Gray, M.B., Ridgway, K.D., Cole, R.B., Srivastava, P., Pequera, N., Pivnik, D.A., 1991. Kinematic history of a foreland uplift from Paleocene synorogenic conglomerate, Beartooth Range, Wyoming and Montana. Geol. Soc. Am. Bull. 103, 1458–1475.

Durdella, M., 2001. Mechanical Modeling of Fault-Related Folds: West Flank of the Bighorn Basin, Wyoming. Purdue University. MS Thesis.

Ebner, M., Koehn, D., Toussaint, R., Renard, F., Schmittbuhl, J., 2009. Stress sensitivity of stylolite morphology. Earth Planet Sci. Lett. 277, 394–398.

Ebner, M., Toussaint, R., Schmittbuhl, J., Koehn, D., Bons, P., 2010. Anisotropic scaling of tectonic stylolites: a fossilized signature of the stress field? J. Geophys. Res. 115, B06403.

Ellis, G.S., Said-Ahmad, W., Lillis, P.G., Shawar, L., Amrani, A., 2017. Effects of thermal maturation and thermochemical sulfate reduction on compound-specific sulfur isotopic compositions of organosulfur compounds in Phosphoria oils from the Bighorn Basin, USA. Org. Geochem. 103, 63–78.

English, J.M., Johnston, S.T., Wang, K., 2003. Thermal modelling of the Laramide orogeny: testing the flat-slab subduction hypothesis. Earth Planet Sci. Lett. 214, 619–632.

Erslev, E.A., Koenig, N.V., 2009. Three-dimensional kinematics of Laramide, basement-involved Rocky Mountain deformation, USA: insights from minor faults and GIS-enhanced structure maps. Geol. Soc. Am. Mem. 204, 125–150.

Fall, A., Eichhubl, P., Cumella, S.P., Bodnar, R.J., Laubach, S.E., Becker, S.P., 2012. Testing the basin-centered gas accumulation model using fluid inclusion observations: southern Piceance Basin, Colorado. AAPG (Am. Assoc. Pet. Geol.) Bull. 96, 2297–2318.

Finkel, E.A., Wilkinson, B.H., 1990. Stylolitization as source of cement in Mississippian salem limestone, west-central Indiana (1). AAPG (Am. Assoc. Pet. Geol.) Bull. 74, 174–186.

Fletcher, R.C., Pollard, D.D., 1981. Anticrack model for pressure solution surfaces. Geology 9, 419–424.

Fox, J., Dolton, G., 1996. Petroleum geology of the Bighorn Basin, north-central Wyoming and south-central Montana. Resources of the Bighorn Basin. Wyoming Geological Association Guidebook, pp. 19–39.

Gottardi, R., Adams, L.M., Borrok, D., Teixeira, B., 2019. Hydrocarbon source rock characterization, burial history, and thermal maturity of the Steele, Niobrara and Mowry Formations at Teapot Dome, Wyoming. Mar. Petrol. Geol. 100, 326–340.

Guidish, T., Kendall, C.S.C., Lerche, I., Toth, D., Yarzab, R., 1985. Basin evaluation using burial history calculations: an overview. AAPG (Am. Assoc. Pet. Geol.) Bull. 69, 92–105.

Heap, M., Reuschlé, T., Baud, P., Renard, F., Iezzi, G., 2018. The permeability of stylolite-bearing limestone. J. Struct. Geol. 116, 81–93.

Koehn, D., Ebner, M., Renard, F., Toussaint, R., Passchier, C.W., 2012. Modelling of stylolite geometries and stress scaling. Earth Planet Sci. Lett. 341–344, 104–113.

Koehn, D., Renard, F., Toussaint, R., Passchier, C., 2007. Growth of stylolite teeth patterns depending on normal stress and finite compaction. Earth Planet Sci. Lett. 257, 582–595.

Koehn, D., Rood, M.P., Beaudoin, N., Chung, P., Bons, P.D., Gomez-Rivas, E., 2016. A new stylolite classification scheme to estimate compaction and local permeability variations. Sediment. Geol. 346, 60–71.

Lacombe, O., 2007. Comparison of paleostress magnitudes from calcite twins with contemporary stress magnitudes and frictional sliding criteria in the continental crust : mechanical implications. J. Struct. Geol. 29, 86–99.

Lacombe, O., Bellahsen, N., 2016. Thick-skinned tectonics and basement-involved fold–thrust belts: insights from selected Cenozoic orogens. Geol. Mag. 153, 763–810.

Lacombe, O., Malandain, J., Vilasi, N., Amrouch, K., Roure, F., 2009. From paleostresses to paleoburial in fold–thrust belts: preliminary results from calcite twin analysis in the Outer Albanides. Tectonophysics 475, 128–141.

Laronne Ben-Itzhak, L., Aharonov, E., Karcz, Z., Kaduri, M., Toussaint, R., 2014. Sedimentary stylolite networks and connectivity in limestone: large-scale field observations and implications for structure evolution. J. Struct. Geol. 63, 106–123.

Lovely, P., Zahasky, C., Pollard, D.D., 2010. Fold geometry at Sheep Mountain anticline, Wyoming, constructed using airborne laser swath mapping data, outcrop-scale geologic mapping, and numerical interpolation. J. Geophys. Res. 115, B12.

Manger, G.E., 1963. Porosity and Bulk Density of Sedimentary Rocks, 1144-E. USGS Bulletin, p. 55.

Marshak, S., Engelder, T., 1985. Development of cleavage in limestones of a fold-thrust belt in eastern New York. J. Struct. Geol. 7 (3–4), 345–359.

Marshak, S., Karlstrom, K., Timmons, J.M., 2000. Inversion of Proterozoic extensional faults: an explanation for the pattern of Laramide and Ancestral Rockies intracratonic deformation, United States. Geology 28, 735–738.

Martín-Martín, J.D., Gomez-Rivas, E., Gómez-Gras, D., Travé, A., Ameneiro, R., Koehn, D., Bons, P.D., 2018. Activation of stylolites as conduits for overpressured fluid flow in dolomitized platform carbonates. Geol. Soc. Lond. Spec. Publ. 459, 157–176.

May, S.R., Gray, G.G., Summa, L.L., Stewart, N.R., Gehrels, G.E., Pecha, M.E., 2013. Detrital zircon geochronology from the Bighorn Basin, Wyoming, USA: implications for tectonostratigraphic evolution and paleogeography. Geol. Soc. Am. Bull. 125, 1403–1422.

Naeser, N.D., McCulloh, T.H., 2012. Thermal History of Sedimentary Basins: Methods and Case Histories. Springer Science & Business Media.

Neely, T.G., Erslev, E.A., 2009. The interplay of fold mechanisms and basement weaknesses at the transition between Laramide basement-involved arches, north-central Wyoming, USA. J. Struct. Geol. 31, 1012–1027.

Railsback, L.B., 1993. Contrasting styles of chemical compaction in the upper Pennsylvanian Dennis limestone in the Midcontinent region, USA. J. Sediment. Res. 63, 61–72.

Renard, F., 2004. Three-dimensional roughness of stylolites in limestones. J. Geophys. Res. 109, B03209.

Renard, F., Dysthe, D., Feder, J., Bjørlykke, K., Jamtveit, B., 2001. Enhanced pressure solution creep rates induced by clay particles: experimental evidence in salt aggregates. Geophys. Res. Lett. 28, 1295–1298.

Rolland, A., Toussaint, R., Baud, P., Conil, N., Landrein, P., 2014. Morphological analysis of stylolites for paleostress estimation in limestones. Int. J. Rock Mech. Min. Sci. 67, 212–225.

Rolland, A., Toussaint, R., Baud, P., Schmittbuhl, J., Conil, N., Koehn, D., Renard, F., Gratier, J.-P., 2012. Modeling the growth of stylolites in sedimentary rocks. J. Geophys. Res.: Solid Earth 117, B06403.

Roure, F., Andriessen, P., Callot, J.-P., Faure, J.-L., Ferket, H., Gonzales, E., Guilhaumou, N., Lacombe, O., Malandain, J., Sassi, W., 2010. The use of palaeo-thermo-barometers and coupled thermal, fluid flow and pore-fluid pressure modelling for hydrocarbon and reservoir prediction in fold and thrust belts. Geol. Soc. Lond. Spec. Publ. 348, 87–114.

Schmittbuhl, J., Renard, F., Gratier, J.P., Toussaint, R., 2004. Roughness of stylolites: implications of 3D high resolution topography measurements. Phys. Rev. Lett. 93, 238501.

Simonsen, I., Hansen, A., Nes, O.M., 1998. Determination of the Hurst exponent by use of wavelet transforms. Phys. Rev. 58, 2779.

Stockdale, P.B., 1922. Stylolites: Their Nature and Origin-Ind. Indiana University, p. 97.

Tavani, S., Storti, F., Lacombe, O., Corradetti, A., Muñoz, J.A., Mazzoli, S., 2015. A review of deformation pattern templates in foreland basin systems and fold-and-thrust belts: implications for the state of stress in the frontal regions of thrust wedges. Earth Sci. Rev. 141, 82–104.

Tavani, S., Storti, F., Muñoz, J.A., 2010. Scaling relationships between stratabound pressure solution cleavage spacing and layer thickness in a folded carbonate multilayer of the Northern Apennines (Italy). J. Struct. Geol. 32, 278–287.

Tissot, B., Pelet, R., Ungerer, P., 1987. Thermal history of sedimentary basins, maturation indices, and kinetics of oil and gas generation. AAPG Bull. 71, 1445–1466.

Toussaint, R., Aharonov, E., Koehn, D., Gratier, J.P., Ebner, M., Baud, P., Rolland, A., Renard, F., 2018. Stylolites: a review. J. Struct. Geol. 114, 163–195.

Varga, R.J., 1993. Rocky Mountain foreland uplifts: products of a rotating stress field or strain partitioning? Geology 21, 1115–1119.

Weil, A.B., Yonkee, W.A., 2012. Layer-parallel shortening across the Sevier fold-thrust belt and Laramide foreland of Wyoming: spatial and temporal evolution of a complex geodynamic system. Earth Planet Sci. Lett. 357–358, 405–420.

Wright, K., Cygan, R.T., Slater, B., 2001. Structure of the (101 [combining macron] 4) surfaces of calcite, dolomite and magnesite under wet and dry conditions. Phys. Chem. Chem. Phys. 3, 839–844.

Yalcin, M., Littke, R., Sachsenhofer, R., 1997. Thermal History of Sedimentary Basins, Petroleum and Basin Evolution. Springer, pp. 71–167.

Yonkee, W.A., Weil, A.B., 2015. Tectonic evolution of the sevier and Laramide belts within the North American Cordillera orogenic system. Earth Sci. Rev. 150, 531–593.